

# Shift-Net: Image Inpainting via Deep Feature Rearrangement

Zhaoyi Yan<sup>1</sup>, Xiaoming Li<sup>1</sup>, Mu Li<sup>2</sup>, Wangmeng Zuo<sup>1\*</sup>, Shiguang Shan<sup>3,4</sup>

<sup>1</sup>School of Computer Science and Technology, Harbin Institute of Technology, Harbin, China

<sup>2</sup>Department of Computing, The Hong Kong Polytechnic University, Hong Kong, China

<sup>3</sup>Key Lab of Intelligent Information Processing of Chinese Academy of Sciences (CAS),  
Institute of Computing Technology, CAS, Beijing 100190, China

<sup>4</sup>CAS Center for Excellence in Brain Science and Intelligence Technology

yanzhaoyi@outlook.com, csxmli@hit.edu.cn, csmuli@comp.polyu.edu.hk,

wmzuo@hit.edu.cn, sgshan@ict.ac.cn

## Abstract

Deep convolutional networks (CNNs) have exhibited their potential in image inpainting for producing plausible results. However, in most existing methods, e.g., context encoder, the missing parts are predicted by propagating the surrounding convolutional features through a fully connected layer, which intends to produce semantically plausible but blurry result. In this paper, we introduce a special shift-connection layer to the U-Net architecture, namely Shift-Net, for filling in missing regions of any shape with sharp structures and fine-detailed textures. To this end, the encoder feature of the known region is shifted to serve as an estimation of the missing parts. A guidance loss is introduced on decoder feature to minimize the distance between the decoder feature after fully connected layer and the ground truth encoder feature of the missing parts. With such constraint, the decoder feature in missing region can be used to guide the shift of encoder feature in known region. An end-to-end learning algorithm is further developed to train the Shift-Net. Experiments on the Paris StreetView and Places datasets demonstrate the efficiency and effectiveness of our Shift-Net in producing sharper, fine-detailed, and visually plausible results.

## 1. Introduction

Image inpainting is the process of filling in missing regions with plausible hypothesis, and can be used in many real world applications such as removing distracting objects, repairing corrupted or damaged parts, and completing occluded regions. For example, when taking a photo, rare is the case that you are satisfied with what you get directly. Distracting scene elements, such as irrelevant people

\*Corresponding author.

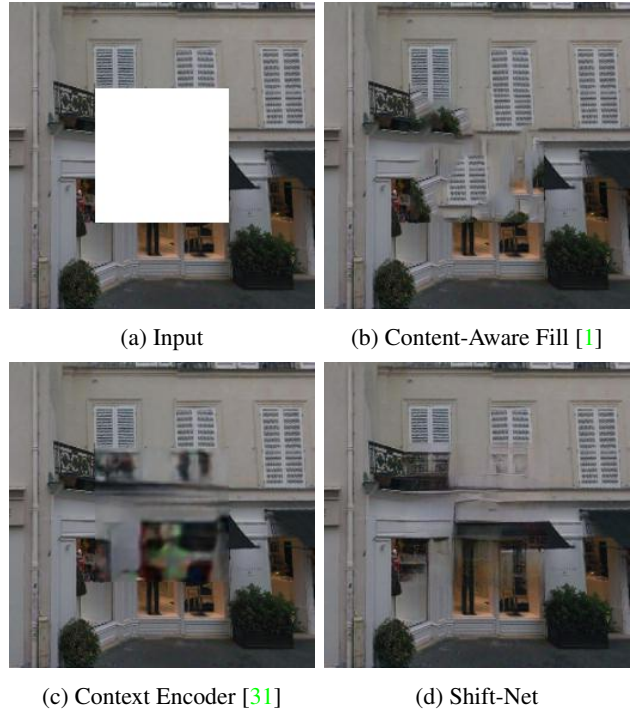


Figure 1: Qualitative comparison of inpainting methods. Given (a) an image with a missing region, we present the inpainting results by (b) Content-Aware Fill [1], (c) context encoder [31], and (d) our Shift-Net.

or disturbing objects, generally are inevitable but unwanted by the users. Fortunately, image inpainting can serve as a remedy to remove these elements and fill in with desirable content.

Despite decades of studies, image inpainting remains a very challenging problem in computer vision and graphics. In general, there are two requirements for the image inpainting result: (i) global semantic structure and (ii) fine de-

tailed textures. Classical exemplar-based inpainting methods, *e.g.*, PatchMatch [2], gradually synthesize the content of missing parts by searching similar patches from known region. Even such methods are promising in filling high-frequency texture details, they fail in capturing the global structure of the image (See Fig. 1b). In contrast, deep convolutional networks (CNNs) have also been suggested to predict the missing parts conditioned on its surroundings [31, 47]. Benefited from large scale training data, they can produce semantically plausible inpainting result. However, the existing CNN-based methods usually complete the missing parts by propagating the surrounding convolutional features through a fully connected layer (*i.e.*, bottleneck), making the inpainting results sometimes lack of fine texture details and blurry. The introduction of adversarial loss is helpful in improving the sharpness of the result, but cannot address this issue essentially (see Fig. 1c).

In this paper, we present a novel CNN, namely Shift-Net, to take into account the advantages of both exemplar-based and CNN-based methods for image inpainting. Our Shift-Net adopts the U-Net architecture by adding a special shift-connection layer. In exemplar-based inpainting [5], the patch-based replication and filling process are iteratively performed to grow the texture and structure from the known region to the missing parts. And the patch processing order plays a key role in yielding plausible inpainting result [25, 46]. We note that CNN is effective in predicting the image structure and semantics of the missing parts. Guided by the salient structure produced by CNN, the filling process in our Shift-Net can be finished concurrently by introducing a shift-connection layer to connect the encoder feature of known region and the decoder feature of missing parts. Thus, our Shift-Net inherits the advantages of exemplar-based and CNN-based methods, and can produce inpainting result with both plausible semantics and fine detailed textures.

Several losses are suggested to guide the shift operation and to learn the network parameters. To ensure that the decoder feature can serve as a good guidance, a guidance loss is introduced to enforce the decoder feature be close to the ground truth encoder feature. Moreover,  $\ell_1$  and adversarial losses are also considered to reconstruct the missing parts and restore more detailed textures. By minimizing the target objective, our Shift-Net can be end-to-end learned with a training set. Extensive experiments are conducted on the Paris StreetView dataset, the Places dataset, and real images. The results show that our Shift-Net can handle missing regions with any shape, and is effective in producing sharper, fine-detailed, and visually plausible results (See Fig. 1d).

Besides, Yang *et al.* [47] also suggest a neural patch synthesis (NPS) approach to incorporating CNN-based with exemplar-based methods. Their method includes two

stages, where an encoder-decoder network is used to generate an initial estimation in the first stage. By considering both global content and texture losses, a joint optimization model on VGG-19 [38] is minimized to generate the fine-detailed result in the second stage. Even Yang *et al.* [47] yields encouraging result, it is very time-consuming and takes about 40,000 millisecond (ms) to process an image with size of  $256 \times 256$ . In contrast, our Shift-Net can achieve comparable or better result (See Fig. 5 for several examples) and only takes 82 ms. Taking both effectiveness and efficiency into account, our Shift-Net can provide a better solution to combine exemplar-based and CNN-based inpainting for improving performance.

To sum up, the main contribution of this work is three-fold:

1. By introducing the shift-connection layer to U-Net, a novel Shift-Net architecture is developed to efficiently combine CNN-based and exemplar-based inpainting.
2. The guidance, reconstruction, and adversarial losses are introduced to train our Shift-Net. Even with the deployment of shift operation, all the network parameters can be learned in an end-to-end manner.
3. Our Shift-Net achieves state-of-the-art results in comparison with [2, 31, 47] and performs favorably in generating fine-detailed textures and visually plausible results.

## 2. Related Work

In this section, we briefly review the work on each of the three sub-fields, *i.e.*, exemplar-based inpainting, CNN-based inpainting, and style transfer, and specially focus on those relevant to this work.

### 2.1. Exemplar-based inpainting

In exemplar-based inpainting [2, 3, 5, 7, 9, 17, 18, 22, 23, 25, 32, 37, 39, 43, 44, 46], the completion is conducted from the exterior to the interior of the missing part by searching and copying best matching patches from the known region. For fast patch search, Barnes *et al.* suggest a PatchMatch algorithm [2] to exploit the image coherency, and generalize it for finding k-nearest neighbors [3]. Exemplar-based inpainting is superior in synthesizing textures, but is not well suited for preserving edges and structures. For better recovery of image structure, several patch priority measures have been proposed to fill in structural patches first [5, 25, 46]. Global image coherence has also been introduced to the Markov random field (MRF) framework for improving visual quality [22, 32, 43]. However, these methods only work well on images with simple structures, and may fail in handling images with complex objects and scenes. Besides, in most exemplar-based inpainting methods [22, 23, 32], the

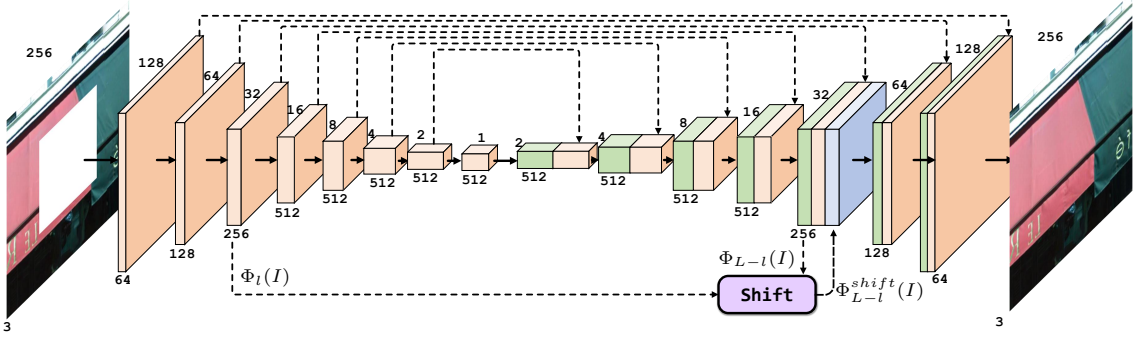


Figure 2: The architecture of our model. We add the shift-connection layer at the resolution of  $32 \times 32$ .

missing part is recovered as the shift representation of the known region in pixel/region level, which also motivates our shift operation on convolution feature representation.

## 2.2. CNN-based inpainting

Recently, deep CNNs have achieved great success in image inpainting. Originally, CNN-based inpainting is confined to small and thin masks [21, 34, 45]. Phatak *et al.* [31] present an encoder-decoder (*i.e.*, context encoder) network to predict the missing parts, where an adversarial loss is adopted in training to improve the visual quality of the inpainted image. Context encoder completes the input image with only one forward-pass. Even it is effective in capturing image semantics and global structure, it still performs poor in generating fine-detailed textures. Other network architecture, *e.g.*, U-Net [35], has been employed to image translation [50] and can also be adopted in image inpainting [16]. Semantic image inpainting is introduced to fill in the missing part conditioned on the known region for images from a specific semantic class [48]. In order to obtain globally consistent result with locally realistic details, global and local discriminators have been proposed in image inpainting [15] and face completion [28]. For better recovery of fine details, multi-scale neural patch synthesis is presented to combine exemplar-based and CNN-based inpainting [47].

## 2.3. Style transfer

Image inpainting can be treated as an extension of style transfer, where both the content and style (texture) of missing part are estimated and transferred from the known region. In the recent few years, style transfer [4, 8, 10, 11, 13, 19, 27, 29, 40] has been an active research topic. Gatys *et al.* [10] show that we can transfer style and texture of the style image to the content image by solving an optimization objective defined on an existing CNN. Instead of the Gram matrix, Li *et al.* [27] apply the MRF regularizer to style transfer to suppress distortions and smears. In [4], local matching is performed on the convolution layer of the pre-trained network to combine content and style, and an in-

verse network is then deployed to generate the image from feature representation.

## 3. Method

Given an input image  $I$ , image inpainting aims to restore the ground truth image  $I^{gt}$  by filling in the missing part. To this end, we adopt U-Net as the baseline network. By incorporating with guidance loss and shift operation, we develop a novel Shift-Net for better recovery of semantic structure and fine-detailed textures. In the following, we first introduce the guidance loss and Shift-Net, and then describe the model objective and learning algorithm.

### 3.1. Guidance loss on decoder feature

The U-Net consists of an encoder and a symmetric decoder, where skip connection is introduced to concatenate the features from each layer of encoder and those of the corresponding layer of decoder. Such skip connection makes it convenient to utilize the information before and after bottleneck, which is valuable for image inpainting and other low level vision tasks in capturing localized visual details [16, 50]. The architecture of the U-Net adopted in this work is shown in Fig. 2. Please refer to the supplementary material for more details on network parameters.

For image inpainting, the U-Net possesses more characteristics which are useful in improving completion result. Let  $\Omega$  be the missing region and  $\bar{\Omega}$  be the known region. Given a U-Net of  $L$  layers,  $\Phi_l(I)$  is used to denote the encoder feature of the  $l$ -th layer, and  $\Phi_{L-l}(I)$  the decoder feature of the  $(L-l)$ -th layer. For the end of recovering  $I^{gt}$ , we expect that  $\Phi_l(I)$  and  $\Phi_{L-l}(I)$  convey almost all the information in  $\Phi_l(I^{gt})$ . For any location  $\mathbf{y} \in \Omega$ , we have  $(\Phi_l(I))_{\mathbf{y}} \approx 0$ . Thus,  $(\Phi_{L-l}(I))_{\mathbf{y}}$  should convey equivalent information of  $(\Phi_l(I^{gt}))_{\mathbf{y}}$ .

In this work, we suggest to explicitly model the relationship between  $(\Phi_{L-l}(I))_{\mathbf{y}}$  and  $(\Phi_l(I^{gt}))_{\mathbf{y}}$  by introducing

the following guidance loss,

$$\mathcal{L}_g = \sum_{\mathbf{y} \in \Omega} \left\| (\Phi_{L-l}(I))_{\mathbf{y}} - (\Phi_l(I^{gt}))_{\mathbf{y}} \right\|_2^2. \quad (1)$$

We note that  $(\Phi_l(I))_{\mathbf{x}} \approx (\Phi_l(I^{gt}))_{\mathbf{x}}$  for any  $\mathbf{x} \in \bar{\Omega}$ . Thus the guidance loss is only defined on  $\mathbf{y} \in \Omega$  to make  $(\Phi_{L-l}(I))_{\mathbf{y}} \approx (\Phi_l(I^{gt}))_{\mathbf{y}}$ . By concatenating  $\Phi_l(I)$  and  $\Phi_{L-l}(I)$ , all information in  $\Phi_l(I^{gt})$  can be approximately obtained.

Experiment on deep feature visualization is further conducted to illustrate the relation between  $(\Phi_{L-l}(I))_{\mathbf{y}}$  and  $(\Phi_l(I^{gt}))_{\mathbf{y}}$ . For visualizing  $\{(\Phi_l(I^{gt}))_{\mathbf{y}} | \mathbf{y} \in \Omega\}$ , we adopt the method [30] by solving an optimization problem

$$H^{gt} = \arg \min_H \sum_{\mathbf{y} \in \Omega} \left\| (\Phi_l(H))_{\mathbf{y}} - (\Phi_l(I^{gt}))_{\mathbf{y}} \right\|_2^2. \quad (2)$$

Analogously,  $\{(\Phi_{L-l}(I))_{\mathbf{y}} | \mathbf{y} \in \Omega\}$  is visualized by

$$H^{de} = \arg \min_H \sum_{\mathbf{y} \in \Omega} \left\| (\Phi_l(H))_{\mathbf{y}} - (\Phi_{L-l}(I))_{\mathbf{y}} \right\|_2^2. \quad (3)$$

Fig. 3(b)(c) show the visualization results of  $H^{gt}$  and  $H^{de}$ . With the introduction of guidance loss, obviously  $H^{de}$  can serve as a reasonable estimation of  $H^{gt}$ , and U-Net works well in recovering image semantics and structures. However, in compared with  $H^{gt}$  and  $I^{gt}$ , the result  $H^{de}$  is blurry, which is consistent with the poor performance of CNN-based inpainting in recovering fine textures [47]. Finally, we note that the guidance loss is helpful in constructing an explicit relation between  $(\Phi_{L-l}(I))_{\mathbf{y}}$  and  $(\Phi_l(I^{gt}))_{\mathbf{y}}$ . In the next section, we will explain how to utilize such property for better estimation to  $(\Phi_l(I^{gt}))_{\mathbf{y}}$  and enhancing inpainting result.

### 3.2. Shift operation and Shift-Net

In exemplar-based inpainting, it is generally assumed that the missing part is the spatial rearrangement of the pixels/patches in the known region. For each pixel/patch localized at  $\mathbf{y}$  in missing part, exemplar-based inpainting explicitly or implicitly find a shift vector  $\mathbf{u}_{\mathbf{y}}$ , and recover  $(I)_{\mathbf{y}}$  with  $(I)_{\mathbf{y}+\mathbf{u}_{\mathbf{y}}}$ , where  $\mathbf{y} + \mathbf{u}_{\mathbf{y}} \in \bar{\Omega}$  is in the known region. The pixel value  $(I)_{\mathbf{y}}$  is unknown before inpainting. Thus, the shift vectors usually are obtained progressively from the exterior to the interior of the missing part, or by solving a MRF model by considering global image coherence. However, these methods may fail in recovering complex image semantics and structures.

As illustrated in Fig. 4, we introduce a special shift-connection layer in U-Net, which takes  $\Phi_l(I)$  and  $\Phi_{L-l}(I)$  to obtain an updated estimation on  $\Phi_l(I^{gt})$ . For each  $(\Phi_{L-l}(I))_{\mathbf{y}}$  with  $\mathbf{y} \in \Omega$ , its nearest neighbor searching in

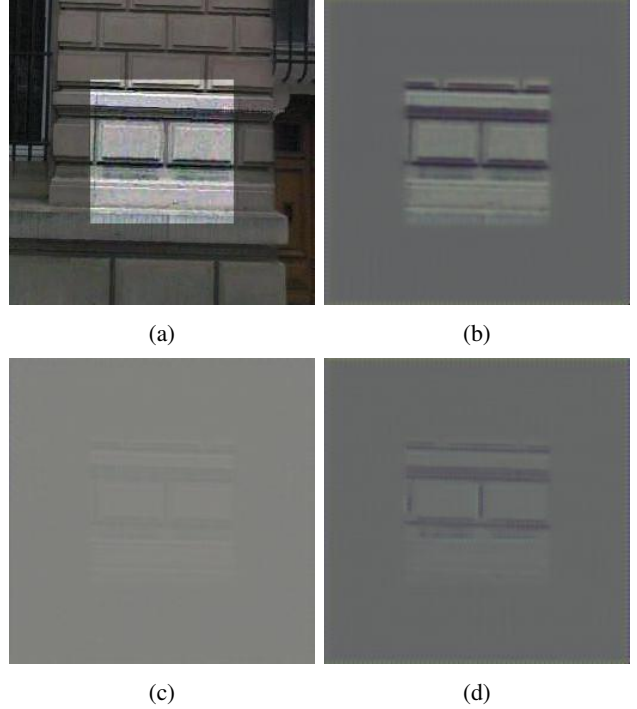


Figure 3: Visualization of features learned by our model. Given (a) an input image, (b) is the visualization of  $(\Phi_l(I^{gt}))_{\mathbf{y}}$  (i.e.,  $H^{gt}$ ), (c) shows the result of  $(\Phi_{L-l}(I))_{\mathbf{y}}$  (i.e.,  $H^{de}$ ) and (d) demonstrates the effect of  $(\Phi_{L-l}^{shift}(I))_{\mathbf{y}}$ .

$(\Phi_l(I))_{\mathbf{x}}$  ( $\mathbf{x} \in \bar{\Omega}$ ) can be independently obtained by,

$$\mathbf{x}^*(\mathbf{y}) = \arg \max_{\mathbf{x} \in \bar{\Omega}} \frac{\langle (\Phi_{L-l}(I))_{\mathbf{y}}, (\Phi_l(I))_{\mathbf{x}} \rangle}{\|(\Phi_{L-l}(I))_{\mathbf{y}}\|_2 \|(\Phi_l(I))_{\mathbf{x}}\|_2}, \quad (4)$$

and the shift vector is defined as  $\mathbf{u}_{\mathbf{y}} = \mathbf{x}^*(\mathbf{y}) - \mathbf{y}$ . Similar to [27], the nearest neighbor searching can be computed as a convolutional layer. Then, we update the estimation of  $(\Phi_l(I^{gt}))_{\mathbf{y}}$  as the spatial rearrangement of the encoder feature  $(\Phi_l(I))_{\mathbf{x}}$ ,

$$(\Phi_{L-l}^{shift}(I))_{\mathbf{y}} = (\Phi_l(I))_{\mathbf{y}+\mathbf{u}_{\mathbf{y}}}. \quad (5)$$

See Fig. 3(d) for visualization. Finally, as shown in Fig. 2, the convolution features  $\Phi_{L-l}(I)$ ,  $\Phi_l(I)$  and  $\Phi_{L-l}^{shift}(I)$  are concatenated and taken as inputs to the  $(L-l+1)$ -th layer, resulting in our Shift-Net.

The shift operation is different with exemplar-based inpainting from several aspects. (i) While exemplar-based inpainting is operated on pixels/patches, shift operation is performed on deep encoder feature which is end-to-end learned from training data. (ii) In exemplar-based inpainting, the shift vectors are obtained either by solving an optimization problem or in particular order. As for shift operation, with the guidance of  $\Phi_{L-l}(I)$ , all the shift vectors can be computed in parallel. (iii) For exemplar-based inpainting, both

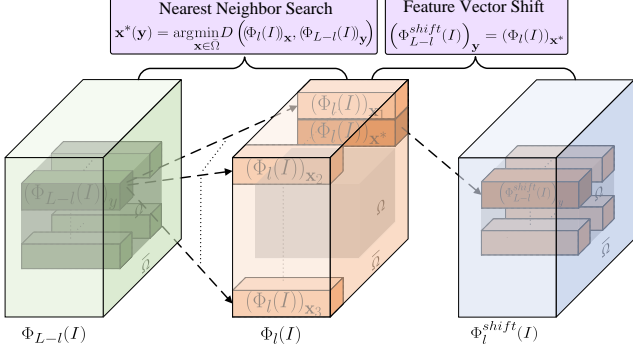


Figure 4: Illustration of the shift operation.

patch processing orders and global image coherence are not sufficient for preserving complex structures and semantics. In contrast, in shift operation  $\Phi_{L-l}(I)$  is learned from large scale data and is more powerful in capturing global semantics. (iv) In exemplar-based inpainting, after obtaining the shift vectors, the completion result can be directly obtained as the shift representation of the known region. As for shift operation, we take the shift representation  $\Phi_{L-l}^{shift}(I)$  together with  $\Phi_{L-l}(I)$  and  $\Phi_l(I)$  as inputs to  $(L-l+1)$ -th layer of U-Net, and adopt a data-driven manner to learn an optimal model for image inpainting. To sum up, even with the introduction of shift-connection layer, all the model parameters in our Shift-Net can be end-to-end learned from training data. Thus, our Shift-Net naturally inherits the advantages of exemplar-based and CNN-based inpainting.

### 3.3. Model objective and learning

#### 3.3.1 Objective

Denote by  $\Phi(I; \mathbf{W})$  the output of our Shift-Net, where  $\mathbf{W}$  is the model parameters to be learned. Besides the guidance loss, the  $\ell_1$  loss and the adversarial loss are also considered to train our Shift-Net. The  $\ell_1$  loss is defined as,

$$\mathcal{L}_{\ell_1} = \|\Phi(I; \mathbf{W}) - I^{gt}\|_1, \quad (6)$$

which is suggested to constrain that the inpainting result should be close to the ground truth image.

Recently, adversarial loss has been adopted in many low level vision [26] and image generation tasks[16, 33], and exhibits its superiority in restoring high-frequency details and photo-realistic textures. As for image inpainting, we use  $p_{data}(I^{gt})$  to denote the distribution of the ground truth images, and  $p_{miss}(I)$  to denote the distribution of the input image. The adversarial loss is then defined as,

$$\mathcal{L}_{adv} = \max_D \mathbb{E}_{I^{gt} \sim p_{data}(I^{gt})} [\log D(I^{gt})] \quad (7)$$

$$+ \mathbb{E}_{I \sim p_{miss}(I)} [\log(1 - D(\Phi(I; \mathbf{W})))] \quad (8)$$

where  $D(\cdot)$  denotes the discriminator to predict the probability that an image is from the distribution  $p_{data}(I^{gt})$ .

Taking guidance,  $\ell_1$ , and adversarial losses into account, the overall objective of our Shift-Net is defined as,

$$\mathcal{L} = \mathcal{L}_{\ell_1} + \lambda_g \mathcal{L}_g + \lambda_{adv} \mathcal{L}_{adv}, \quad (9)$$

where  $\lambda_g$  and  $\lambda_{adv}$  are the tradeoff parameters for the guidance and adversarial losses, respectively.

#### 3.3.2 Learning

Given a training set  $\{(I, I^{gt})\}$ , the Shift-Net is trained by minimizing the objective in Eqn. (9) via back-propagation. We note that the Shift-Net and the discriminator are trained in an adversarial manner. The Shift-Net  $\Phi(I; \mathbf{W})$  is updated by minimizing the adversarial loss  $\mathcal{L}_{adv}$ , while the discriminator  $D$  is updated by maximizing  $\mathcal{L}_{adv}$ .

Due to the introduction of shift-connection layer, we should modify the computation of the gradient with respect to the  $l$ -th layer of feature  $F_l = \Phi_l(I)$ . To avoid confusion, we use  $F_l^{skip}$  to denote the feature  $F_l$  after skip connection, and of course we have  $F_l^{skip} = F_l$ . According to Eqn. (5), the relation between  $\Phi_{L-l}^{shift}(I)$  and  $\Phi_l(I)$  can be written as,

$$\Phi_{L-l}^{shift}(I) = \mathbf{P}\Phi_l(I), \quad (10)$$

where  $\mathbf{P}$  denotes the shift matrix of  $\{0, 1\}$ , and there is only one element of 1 in each row of  $\mathbf{P}$ . Thus, the gradient with respect to  $\Phi_l(I)$  consists of three terms,

$$\frac{\partial \mathcal{L}}{\partial F_l} = \frac{\partial \mathcal{L}}{\partial F_l^{skip}} + \frac{\partial \mathcal{L}}{\partial F_{l+1}} \frac{\partial F_{l+1}}{\partial F_l} + \mathbf{P}^T \frac{\partial \mathcal{L}}{\partial \Phi_{L-l}^{shift}(I)}, \quad (11)$$

where the computation of the first two terms are the same with U-Net, and the gradient with respect to  $\Phi_{L-l}^{shift}(I)$  can also be directly computed. Thus, our Shift-Net can also be end-to-end trained to learn the model parameters  $\mathbf{W}$ .

#### 3.4. Implementation

In the previous subsections, we assume that the missing region  $\Omega$  is invariant in all the encoder layers. Actually,  $\Omega$  changes along with the convolution and pooling operations. Denote by  $\Omega^0$  the missing part of the input image, and we should determine  $\Omega^l$  for the  $l$ -th convolutional layer. In our implementation, we introduce a mask image  $M$  with  $(M)_{\mathbf{y}} = 1$  ( $\mathbf{y} \in \Omega$ ) and 0 otherwise. Then, we define a CNN  $\Psi(M)$  that has the same architecture with the encoder but with the network width of 1. All the elements of the filters are  $1/16$ , and we remove all the nonlinearity. Taking  $M$  as input, we obtain the feature of the  $l$ -th layer as  $\Psi_l(M)$ . Then,  $\Omega^l$  is defined as  $\Omega^l = \{\mathbf{y} | (\Psi_l(M))_{\mathbf{y}} \geq T\}$ , where  $T$  is the threshold with  $0 \leq T \leq 1$ . Here we empirically set  $T = 5/16$ .

Our Shift-Net is optimized using the Adam algorithm [20] with a learning rate of  $2 \times 10^{-4}$  and  $\beta_1 = 0.5$ .

The batch size is 1 and the training is stopped after 20 epochs. Data augmentation such as flipping is also adopted during training. The tradeoff parameters are set as  $\lambda_g = 0.1$  and  $\lambda_{adv} = 0.01$ .

## 4. Experiments

We evaluate our method on two datasets: Paris StreetView [6] and six scenes from Places365-Standard dataset [49]. The Paris StreetView contains 14,900 training images and 100 test images. There are 1.6 million training images from 365 scene categories in the Places365-Standard. The scene categories selected from Places365-Standard are *butte*, *canyon*, *field*, *synagogue*, *tundra* and *valley*. Each category has 5,000 training images, 900 test images and 100 validation images. Our model is learned using the training set and tested on the validation set. For both Paris StreetView and Places, we resize each training image to let its minimal length/width be 350, and randomly crop a subimage of size  $256 \times 256$  as input to our model. Moreover, our method is also tested on real images for removing objects and distractors. It takes about one day to train our Shift-Net on an Nvidia Titan X Pascal GPU. All the source codes will be released after the publication of this work.

### 4.1. Comparisons with other algorithms

We compare our results with Photoshop Content-Aware Fill [1] based on [2], Context-Encoders [31], and Multi-scale Neural Patch Synthesis (MNPS) [47]. As Context Encoder only accepts  $128 \times 128$  images, we upsample the results to  $256 \times 256$ . For MNPS [47], we set the pyramid level be 2 to get the resolution of  $256 \times 256$ .

**Evaluation on Paris StreetView and Places** Fig. 5 shows the comparisons of our method with other state-of-the-art approaches on Paris StreetView. Content-Aware Fill [1] is effective in recovering low level textures, but performs slightly worse in handling occlusions with complex structures. Context-Encoders [31] is effective in semantic inpainting, but the results seem blurry and detail-missing due to the effect of bottleneck. MNPS [47] adopts a multi-stage scheme to combine CNN and exemplar-based inpainting, and generally works better than Content-Aware Fill [1] and Context-Encoders [31]. However, the multi-scales in MNPS [47] are not jointly trained, where some adverse effects produced in the first stage may not be eliminated by the subsequent stages. In comparison to the competing methods, our Shift-Net combines CNN and exemplar-based inpainting in an end-to-end manner, and generally is able to generate visual-pleasing results. Moreover, we also note that our Shift-Net is much more efficient than MNPS [47]. Our method consumes only about 80 ms for a  $256 \times 256$  image, which is about  $500\times$  faster than MNPS [47] (about 40 seconds). In addition, we also evaluate our method on the

Places dataset. Please see Fig. 6 for the results. Again our Shift-Net performs favorably in generating fine-detailed, semantically plausible, and realistic images.

**Quantitative evaluation** We also compare our model quantitatively with the competing methods on the Paris StreetView dataset. Table 1 lists the PSNR, SSIM and mean  $\ell_2$  loss of different methods. Our Shift-Net gets better or comparable SSIM with the competing methods. In terms of SSIM and mean  $\ell_2$  loss, our Shift-Net is a little inferior to MNPS [47] but are better than the others. Actually, both PSNR and SSIM are correlated poorly with human assessment of visual quality [12, 14, 24, 36, 42]. Moreover, inpainting aims at generating visual-pleasing results, rather than faithfully recovering the same content of missing parts.

Table 1: Comparison of PSNR, SSIM and mean  $\ell_2$  loss on Paris StreetView dataset.

Method	PSNR	SSIM	Mean $\ell_2$ Loss
Content-Aware Fill [1]	24.48	0.88	0.0500
Context Encoder [31] ( $\ell_2$ + adversarial loss)	26.06	0.88	0.0350
MNPS [47]	<b>27.32</b>	<b>0.91</b>	<b>0.0261</b>
Ours	27.17	<b>0.91</b>	0.0283

**Random mask completion** Our model can also be trained for arbitrary region completion. Fig. 7 shows the results by Content-Aware Fill [1] and our Shift-Net. For texture and smooth regions, both Content-Aware Fill [1] and our Shift-Net perform favorably. While for structural region, our Shift-Net is more effective in filling the cropped regions with context coherent with global content and structures.

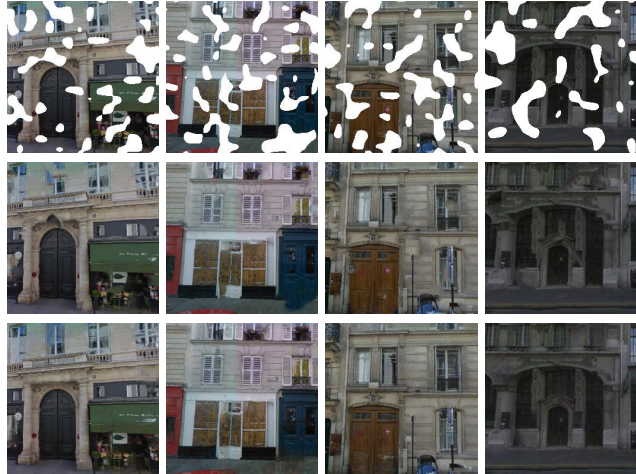


Figure 7: Random region completion. From top to bottom are: Input, Content-Aware Fill [1], and Ours.

### 4.2. Image inpainting in real world

We also evaluate our Shift-Net trained on Paris StreetView for the inpainting of real images by consider-

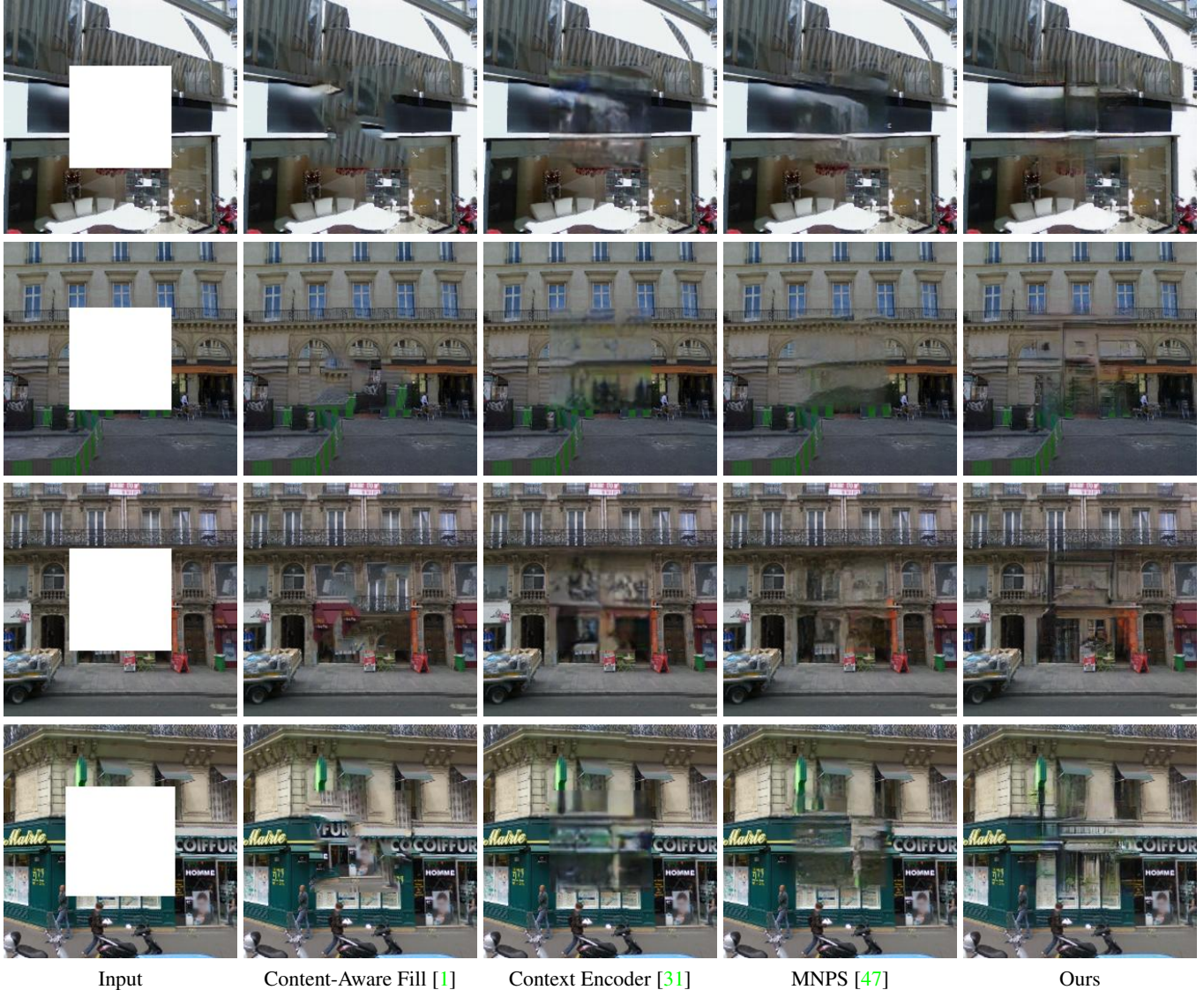


Figure 5: Qualitative comparisons on the Paris StreetView dataset. All images are scaled to  $256 \times 256$ .

ing two types of missing regions: (i) central region, (ii) object removal. From the first row of Fig. 8, one can see that our Shift-Net trained with central mask can be generalized to handle real images. From the second row of Fig. 8, we show the feasibility of using our Shift-Net trained with random mask to remove unwanted objects from the images.

## 5. Internal Analysis of Shift-Net

The main differences between our Shift-Net and the other methods are the introduction of guidance loss and shift-connection layer. Thus, experiments are first conducted to analyze the effect of guidance loss and shift operation. As explained in Sec. 3.4, the missing region  $\Omega^l$  is determined by the threshold  $T$ . So we also evaluate the sensitiveness of our Shift-Net to the threshold. Moreover,

the benefit of shift-connection does not owe to the increase of feature map size or the addition of extra skip connection. To illustrate this, we also compare Shift-Net with a baseline model by substituting the nearest neighbor searching with random shift-connection.

### 5.1. Effect of guidance loss

Two groups of experiments are conducted to evaluate the effect of guidance loss. In the first group of experiments, we add and remove the guidance loss  $\mathcal{L}_g$  for U-Net and our Shift-Net to train the inpainting models. Fig. 10 shows the inpainting results by these four methods. It can be observed that, for both U-Net and Shift-Net the guidance loss is helpful in suppressing artifacts and preserving salient structure.

In the second group of experiments, we evaluate the ef-

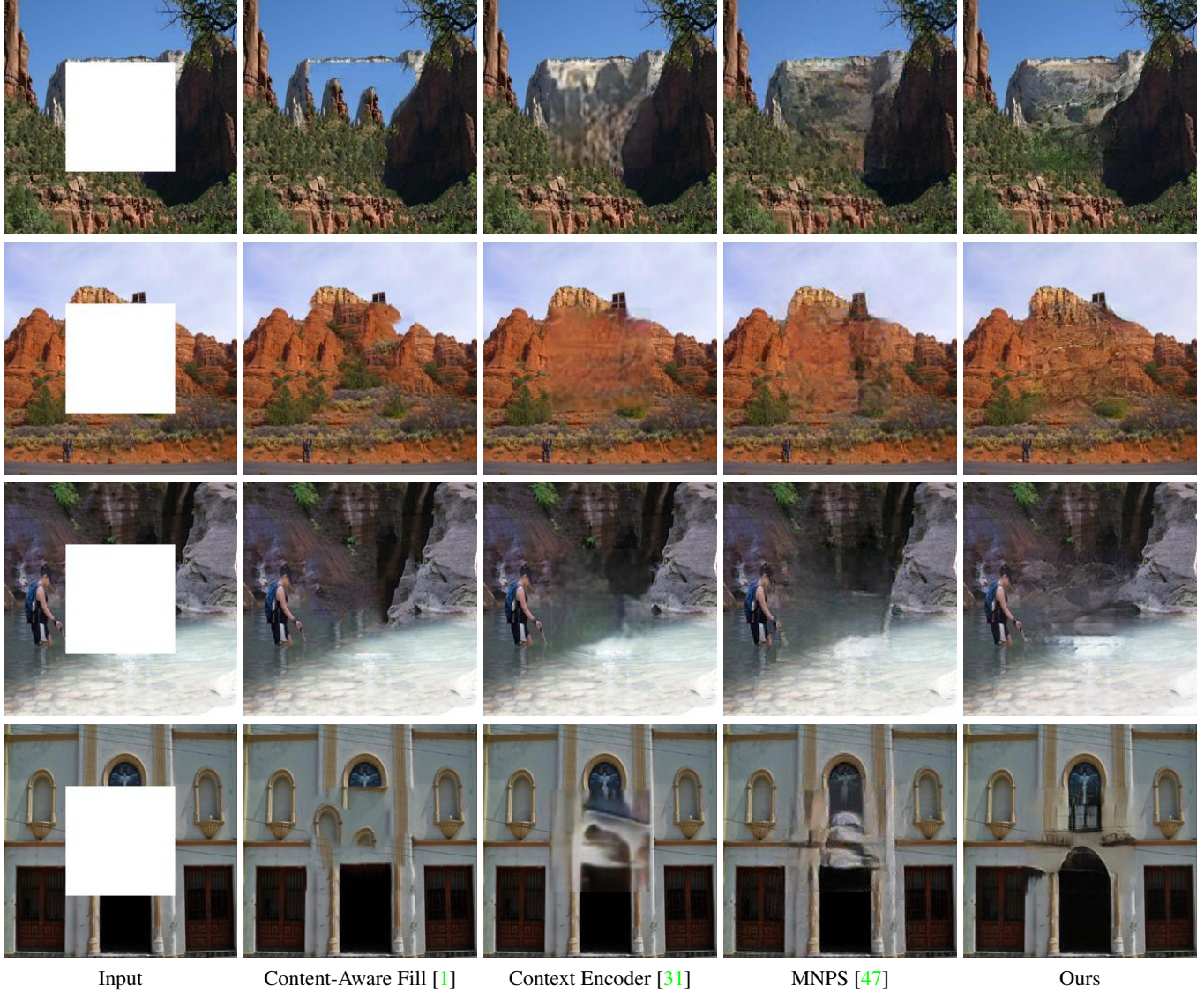


Figure 6: Qualitative comparisons on the Places. All images are scaled to  $256 \times 256$ .

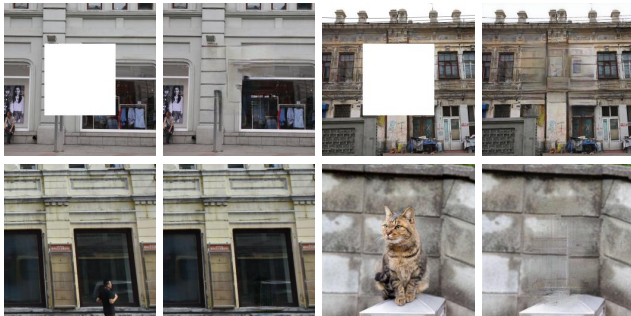


Figure 8: Results on real images. From the top to bottom are: central region inpainting, and object removal.

effect of the tradeoff parameter  $\lambda_g$  for guidance loss. For our Shift-Net, the guidance loss is introduced for both recover-

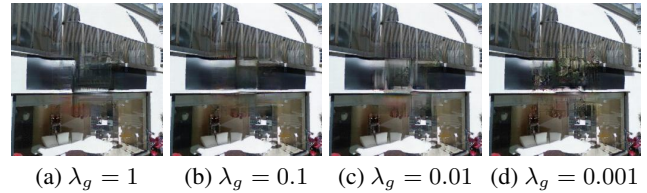


Figure 9: The effect of the tradeoff parameter  $\lambda_g$  of guidance loss.

ing the semantic structure of the missing region and guiding the shift of the encoder feature. To this end, proper tradeoff parameter  $\lambda_g$  should be chosen, where too large or too small  $\lambda_g$  values may be harmful to the inpainting results. Fig. 9 shows the results by setting different  $\lambda_g$  values. When  $\lambda_g$  is small (e.g.,  $\leq 0.01$ ), the decoder feature may not serve as

a suitable guidance to guarantee the correct shift of the encoder feature. From Fig. 9(c)(d), some artifacts and confusing structures can still be observed. When  $\lambda_g$  becomes too large (e.g., = 1), the constraint will be too excessive, and artifacts may also be introduced in the result (see Fig. 9(a)). Thus, we empirically set  $\lambda_g = 0.1$  in all our experiments.

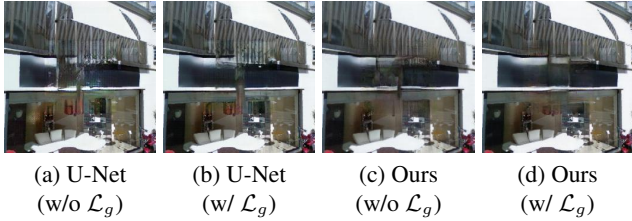


Figure 10: The effect of guidance loss  $\mathcal{L}_g$  in U-Net and our Shift-Net.

### 5.2. Effect of shift operation at different layers

The superiority of Shift-Net against Context-Encoder [31] has demonstrated the effectiveness of shift operation. By comparing the results by U-Net (w/ $\mathcal{L}_g$ ) and Shift-Net (w/ $\mathcal{L}_g$ ) in Fig. 10(b)(d), one can see that shift operation does benefit the preserving of semantics and the recovery of detailed textures. Note that the shift operation can be deployed to different layer, e.g.,  $L - l$ , of the decoder. When  $l$  is smaller, the feature map size goes larger, and more computation time is required to perform the shift operation. When  $l$  is larger, the feature map size becomes smaller, but more more detailed information may lost in the corresponding encoder layer, which may be harmful to recover image details and semantics. Thus, proper  $l$  should be chosen for better tradeoff between computation time and inpainting performance. Fig. 11 shows the results of Shift-Net by adding the shift-connection layer to each of the  $L - 4$ ,  $L - 3$ , and  $L - 2$  layers, respectively. When the shift-connection layer is added to the  $L - 2$  layer, Shift-Net generally works well in producing visually pleasing results, but it takes more time (i.e.,  $\sim 400$  ms per image) to process an image (See Fig. 11(d)). When the shift-connection layer is added to the  $L - 4$  layer, Shift-Net becomes very efficient (i.e.,  $\sim 40$  ms per image) but tends to generate the result with less textures and coarse details (See Fig. 11(b)). By performing the shift operation in  $L - 3$  layer, better tradeoff between efficiency (i.e.,  $\sim 80$  ms per image) and performance can be obtained by Shift-Net (See Fig. 11(c)).

### 5.3. Effect of threshold $T$

Along with the convolution and pooling operations, the mask  $M$  introduced in Sec. 3.4 will not be binary. Thus we introduce a threshold  $T$  ( $0 \leq T \leq 1$ ) to define the missing region  $\Omega^l$ . Fig. 12 shows the results of Shift-Net by setting

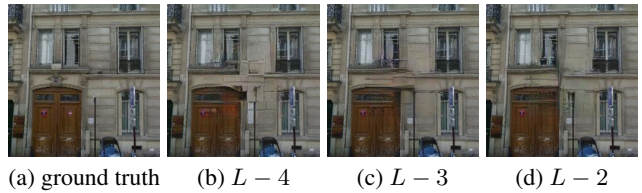


Figure 11: The effect of performing shift operation on different layers  $L - l$ .

$T = 4/16, 5/16, 6/16$ , respectively. It can be seen that Shift-Net is robust to  $T$ , which may be attributed to that we take the shift and encoder, decoder features as the inputs to the  $L - l + 1$  layer. Generally it is more safe to use slightly higher  $T$  values (e.g.,  $5/16, 6/16$ ) in the experiments.

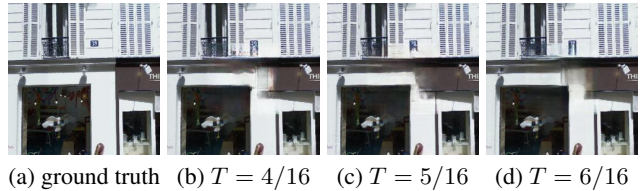


Figure 12: The effect of different thresholds in shift-connection.



Figure 13: From top to bottom are: Shift-Net with random shift-connection and nearest neighbor searching.

### 5.4. Comparison with random shift-connection

Finally, we implement a baseline Shift-Net model by substituting the nearest neighbor searching with random shift-connection. Fig. 13 shows four examples of inpainting results by Shift-Net and baseline model. Compared to the nearest neighbor searching, the results by random shift-connection exhibit more artifacts, distortions, and structure disconnections. Thus, the favorable performance of Shift-Net should owe to the correct shift-operation.

## 6. Conclusion

This paper has proposed a novel architecture, i.e., Shift-Net, for image completion that exhibits fast speed with

promising fine details via deep feature rearrangement. The guidance loss is introduced to enhance the explicit relation between the encoded feature in known region and decoded feature in missing region. By exploiting such relation, the shift operation can be efficiently performed and is effective in improving inpainting performance. Experiments show that our Shift-Net performs favorably in comparison to the state-of-the-art methods, and is effective in generating sharp, fine-detailed and realistic images. In future, more studies will be given to improve the speed of nearest search in the shift operation, introduce multiple shift-connection layers, and investigate other effective solutions to combine CNN and exemplar-based inpainting.

## References

- [1] Content-aware fill. <https://research.adobe.com/project/content-aware-fill>.
- [2] C. Barnes, E. Shechtman, A. Finkelstein, and D. B. Goldman. Patchmatch: a randomized correspondence algorithm for structural image editing. In *ACM Transactions on Graphics (TOG)*, volume 28, page 24. ACM, 2009.
- [3] C. Barnes, E. Shechtman, D. B. Goldman, and A. Finkelstein. The generalized patchmatch correspondence algorithm. In *European Conference on Computer Vision*, pages 29–43. Springer, 2010.
- [4] T. Q. Chen and M. Schmidt. Fast patch-based style transfer of arbitrary style. *arXiv preprint arXiv:1612.04337*, 2016.
- [5] A. Criminisi, P. Perez, and K. Toyama. Object removal by exemplar-based inpainting. In *Computer Vision and Pattern Recognition, 2003. Proceedings. 2003 IEEE Computer Society Conference on*, volume 2, pages II–II. IEEE, 2003.
- [6] C. Doersch, S. Singh, A. Gupta, J. Sivic, and A. Efros. What makes paris look like paris? *ACM Transactions on Graphics*, 31(4), 2012.
- [7] I. Drori, D. Cohen-Or, and H. Yeshurun. Fragment-based image completion. In *ACM Transactions on graphics (TOG)*, volume 22, pages 303–312. ACM, 2003.
- [8] V. Dumoulin, J. Shlens, and M. Kudlur. A learned representation for artistic style. *arXiv preprint arXiv:1610.07629*, 2016.
- [9] A. A. Efros and T. K. Leung. Texture synthesis by non-parametric sampling. In *Computer Vision, 1999. The Proceedings of the Seventh IEEE International Conference on*, volume 2, pages 1033–1038. IEEE, 1999.
- [10] L. A. Gatys, A. S. Ecker, and M. Bethge. A neural algorithm of artistic style. *arXiv preprint arXiv:1508.06576*, 2015.
- [11] L. A. Gatys, A. S. Ecker, M. Bethge, A. Hertzmann, and E. Shechtman. Controlling perceptual factors in neural style transfer. *arXiv preprint arXiv:1611.07865*, 2016.
- [12] P. Hanhart, P. Korshunov, and T. Ebrahimi. Benchmarking of quality metrics on ultra-high definition video sequences. In *Digital Signal Processing (DSP), 2013 18th International Conference on*, pages 1–8. IEEE, 2013.
- [13] X. Huang and S. Belongie. Arbitrary style transfer in real-time with adaptive instance normalization. *arXiv preprint arXiv:1703.06868*, 2017.
- [14] Q. Huynh-Thu and M. Ghanbari. Scope of validity of psnr in image/video quality assessment. *Electronics letters*, 44(13):800–801, 2008.
- [15] S. Iizuka, E. Simo-Serra, and H. Ishikawa. Globally and Locally Consistent Image Completion. *ACM Transactions on Graphics (Proc. of SIGGRAPH 2017)*, 36(4):107:1–107:14, 2017.
- [16] P. Isola, J.-Y. Zhu, T. Zhou, and A. A. Efros. Image-to-image translation with conditional adversarial networks. *arXiv preprint arXiv:1611.07004*, 2016.
- [17] J. Jia and C.-K. Tang. Image repairing: Robust image synthesis by adaptive nd tensor voting. In *Computer Vision and Pattern Recognition, 2003. Proceedings. 2003 IEEE Computer Society Conference on*, volume 1, pages I–I. IEEE, 2003.
- [18] J. Jia and C.-K. Tang. Inference of segmented color and texture description by tensor voting. *IEEE Transactions on Pattern Analysis and Machine Intelligence*, 26(6):771–786, 2004.
- [19] J. Johnson, A. Alahi, and L. Fei-Fei. Perceptual losses for real-time style transfer and super-resolution. In *European Conference on Computer Vision*, pages 694–711. Springer, 2016.
- [20] D. P. Kingma and J. L. Ba. Adam: A method for stochastic optimization. *international conference on learning representations*, 2015.
- [21] R. Köhler, C. Schuler, B. Schölkopf, and S. Harmeling. Mask-specific inpainting with deep neural networks. In *German Conference on Pattern Recognition*, pages 523–534. Springer, 2014.
- [22] N. Komodakis. Image completion using global optimization. In *Computer Vision and Pattern Recognition, 2006 IEEE Computer Society Conference on*, volume 1, pages 442–452. IEEE, 2006.
- [23] N. Komodakis and G. Tziritas. Image completion using efficient belief propagation via priority scheduling and dynamic pruning. *IEEE Transactions on Image Processing*, 16(11):2649–2661, 2007.
- [24] D. Kundu and B. L. Evans. Full-reference visual quality assessment for synthetic images: A subjective study. In *Image Processing (ICIP), 2015 IEEE International Conference on*, pages 2374–2378. IEEE, 2015.
- [25] O. Le Meur, J. Gautier, and C. Guillemot. Exemplar-based inpainting based on local geometry. In *Image Processing (ICIP), 2011 18th IEEE International Conference on*, pages 3401–3404. IEEE, 2011.
- [26] C. Ledig, L. Theis, F. Huszár, J. Caballero, A. Cunningham, A. Acosta, A. Aitken, A. Tejani, J. Totz, Z. Wang, et al. Photo-realistic single image super-resolution using a generative adversarial network. *arXiv preprint arXiv:1609.04802*, 2016.
- [27] C. Li and M. Wand. Combining markov random fields and convolutional neural networks for image synthesis. In *Proceedings of the IEEE Conference on Computer Vision and Pattern Recognition*, pages 2479–2486, 2016.
- [28] Y. Li, S. Liu, J. Yang, and M.-H. Yang. Generative face completion. *arXiv preprint arXiv:1704.05838*, 2017.
- [29] F. Luan, S. Paris, E. Shechtman, and K. Bala. Deep photo style transfer. *arXiv preprint arXiv:1703.07511*, 2017.
- [30] A. Mahendran and A. Vedaldi. Understanding deep image representations by inverting them. In *Proceedings of the*

- IEEE conference on computer vision and pattern recognition*, pages 5188–5196, 2015.
- [31] D. Pathak, P. Krahenbuhl, J. Donahue, T. Darrell, and A. A. Efros. Context encoders: Feature learning by inpainting. In *Proceedings of the IEEE Conference on Computer Vision and Pattern Recognition*, pages 2536–2544, 2016.
- [32] Y. Pritch, E. Kav-Venaki, and S. Peleg. Shift-map image editing. In *Computer Vision, 2009 IEEE 12th International Conference on*, pages 151–158. IEEE, 2009.
- [33] A. Radford, L. Metz, and S. Chintala. Unsupervised representation learning with deep convolutional generative adversarial networks. *arXiv preprint arXiv:1511.06434*, 2015.
- [34] J. S. Ren, L. Xu, Q. Yan, and W. Sun. Shepard convolutional neural networks. In *Advances in Neural Information Processing Systems*, pages 901–909, 2015.
- [35] O. Ronneberger, P. Fischer, and T. Brox. U-net: Convolutional networks for biomedical image segmentation. In *Medical Image Computing and Computer-Assisted Intervention (MICCAI)*, 2015.
- [36] H. R. Sheikh, M. F. Sabir, and A. C. Bovik. A statistical evaluation of recent full reference image quality assessment algorithms. *IEEE Transactions on image processing*, 15(11):3440–3451, 2006.
- [37] D. Simakov, Y. Caspi, E. Shechtman, and M. Irani. Summarizing visual data using bidirectional similarity. In *Computer Vision and Pattern Recognition, 2008. CVPR 2008. IEEE Conference on*, pages 1–8. IEEE, 2008.
- [38] K. Simonyan and A. Zisserman. Very deep convolutional networks for large-scale image recognition. *arXiv preprint arXiv:1409.1556*, 2014.
- [39] J. Sun, L. Yuan, J. Jia, and H.-Y. Shum. Image completion with structure propagation. *ACM Transactions on Graphics (ToG)*, 24(3):861–868, 2005.
- [40] D. Ulyanov, V. Lebedev, A. Vedaldi, and V. S. Lempitsky. Texture networks: Feed-forward synthesis of textures and stylized images. In *ICML*, pages 1349–1357, 2016.
- [41] D. Ulyanov, A. Vedaldi, and V. Lempitsky. Instance normalization: The missing ingredient for fast stylization. *arXiv preprint arXiv:1607.08022*, 2016.
- [42] Z. Wang and A. C. Bovik. Mean squared error: Love it or leave it? a new look at signal fidelity measures. *IEEE signal processing magazine*, 26(1):98–117, 2009.
- [43] Y. Wexler, E. Shechtman, and M. Irani. Space-time video completion. In *Computer Vision and Pattern Recognition, 2004. CVPR 2004. Proceedings of the 2004 IEEE Computer Society Conference on*, volume 1, pages I–I. IEEE, 2004.
- [44] Y. Wexler, E. Shechtman, and M. Irani. Space-time completion of video. *IEEE Transactions on pattern analysis and machine intelligence*, 29(3), 2007.
- [45] J. Xie, L. Xu, and E. Chen. Image denoising and inpainting with deep neural networks. In *Advances in Neural Information Processing Systems*, pages 341–349, 2012.
- [46] Z. Xu and J. Sun. Image inpainting by patch propagation using patch sparsity. *IEEE transactions on image processing*, 19(5):1153–1165, 2010.
- [47] C. Yang, X. Lu, Z. Lin, E. Shechtman, O. Wang, and H. Li. High-resolution image inpainting using multi-scale neural patch synthesis. In *The IEEE Conference on Computer Vision and Pattern Recognition (CVPR)*, July 2017.
- [48] R. A. Yeh, C. Chen, T. Y. Lim, A. G. Schwing, M. Hasegawa-Johnson, and M. N. Do. Semantic image inpainting with deep generative models. In *Proceedings of the IEEE Conference on Computer Vision and Pattern Recognition*, pages 5485–5493, 2017.
- [49] B. Zhou, A. Lapedriza, A. Khosla, A. Oliva, and A. Torralba. Places: A 10 million image database for scene recognition. *IEEE Transactions on Pattern Analysis and Machine Intelligence*, 2017.
- [50] J.-Y. Zhu, T. Park, P. Isola, and A. A. Efros. Unpaired image-to-image translation using cycle-consistent adversarial networks. *arXiv preprint arXiv:1703.10593*, 2017.

## A. Details on Shift-Net

**Architecture of generative model G** For the generative model of our Shift-Net, we adopt the architecture of U-Net proposed in [16, 33]. Each convolution/deconvolution layer is followed by instance normalization [41]. The encoder part of  $G$  is a stack of Convolution-InstanceNorm-LeakyReLU layers, while the decoder part consists of a series of Deconvolution-InstanceNorm-ReLU layers. In training, we zero out the biases of all convolution and deconvolution layers in the generative model.  $L$  denotes the total number of convolution/deconvolution layers in our model. We add guidance loss constraint and shift operation in the layer  $L - 3$ , which results in the concatenated features of  $\Phi_{L-3}(I)$ ,  $\Phi_3(I)$  and  $\Phi_{L-3}^{shift}(I)$  as inputs of the adjacent deconvolution. Details about the architecture of our generative model  $G$  is shown in Table 2. It is remarkable that we do not apply InstanceNorm on the bottleneck layer. The activation map of the bottleneck layer is  $1 \times 1$ , which means we only get one activation per convolutional filter. As we train our network with batchsize 1, activations will be zeroed out once InstanceNorm is applied on the bottleneck layer. You may refer to pix2pix<sup>1</sup> for more explanation.

**Architecture of discriminative network D**  $D$  shares the similar design pattern with the encoder part of  $G$ , however, is only 5-convolutional-layer network. We exclusively use convolutional layers with filters of size  $4 \times 4$  pixels with varying stride lengths to reduce the spatial dimension of the input down to a size of  $30 \times 30$  where we append sigmoid activation at the final output. InstanceNorm is not applied to the first convolutional layer, and we use leaky ReLU with slope of 0.2 for activations except for the sigmoid in the last layer. See Table 3 for more details.

## B. More comparisons and object removals

### B.1. Comparisons on Paris StreetView dataset

More comparisons with Context-Encoders [31], Content-Aware-Fill [1] and MNPS [47] on Paris StreetView dataset [6] are also conducted. Please refer to Fig. 14, Fig. 15 and Fig. 16 for more results. Our Shift-Net outperforms other state-of-the-art approaches in both structural consistency and image clarity. Both global structure and fine details can be preserved in our model, however, other methods either do badly in generating clear, realistic details or lack global structure consistency.

<sup>1</sup><https://github.com/phillipi/pix2pix/commit/b50f5dc>

Table 2: The architecture of the  $G$  network. “IN” represents InstanceNorm and “LReLU” donates leaky ReLU with the slope of 0.2. Guidance loss and shift-connection layer are added in the layer of  $L - 3$ .

The architecture of generative model $G$	
<b>Input:</b> Image ( $256 \times 256 \times 3$ )	
[Layer 1]	Conv. (4, 4, 64), stride=2;
[Layer 2]	LReLU; Conv. (4, 4, 128), stride=2; IN;
[Layer 3]	LReLU; Conv. (4, 4, 256), stride=2; IN;
[Layer 4]	LReLU; Conv. (4, 4, 512), stride=2; IN;
[Layer 5]	LReLU; Conv. (4, 4, 512), stride=2; IN;
[Layer 6]	LReLU; Conv. (4, 4, 512), stride=2; IN;
[Layer 7]	LReLU; Conv. (4, 4, 512), stride=2; IN;
[Layer 8]	LReLU; Conv. (4, 4, 512), stride=2;
[Layer 9]	ReLU; DeConv. (4, 4, 512), stride=2; IN;
	Concatenate(Layer 9, Layer 7);
[Layer 10]	DeConv. (4, 4, 512), stride=2; IN;
	Concatenate(Layer 10, Layer 6); ReLU;
[Layer 11]	DeConv. (4, 4, 512), stride=2; IN;
	Concatenate(Layer 11, Layer 5); ReLU;
[Layer 12]	DeConv. (4, 4, 512), stride=2; IN;
	Concatenate(Layer 12, Layer 4); ReLU;
[Layer 13]	DeConv. (4, 4, 256), stride=2; IN;
	Concatenate(Layer 13, Layer 3); ReLU;
[Layer 14]	<b>Guidance loss layer;</b>
[Layer 15]	<b>Shift-connection layer;</b>
[Layer 16]	DeConv. (4, 4, 128), stride=2; IN;
	Concatenate(Layer 16, Layer 2); ReLU;
[Layer 17]	DeConv. (4, 4, 64), stride=2; IN;
	Concatenate(Layer 17, Layer 1); ReLU;
[Layer 18]	ReLU; DeConv. (4, 4, 3), stride=2; Tanh;
<b>Output:</b> Final result ( $256 \times 256 \times 3$ )	

Table 3: The architecture of the discriminative network. “IN” represents InstanceNorm and “LReLU” donates leaky ReLU with the slope of 0.2.

The architecture of discriminative model $D$	
<b>Input:</b> Image ( $256 \times 256 \times 3$ )	
[layer 1]	Conv. (4, 4, 64), stride=2; LReLU;
[layer 2]	Conv. (4, 4, 128), stride=2; IN; LReLU;
[layer 3]	Conv. (4, 4, 256), stride=2; IN; LReLU;
[layer 4]	Conv. (4, 4, 512), stride=1; IN; LReLU;
[layer 5]	Conv. (4, 4, 1), stride=1; Sigmoid;
<b>Output:</b> Real or Fake ( $30 \times 30 \times 1$ )	

## B.2. More object removal on real images by our Shift-Net

We apply our model trained on Paris StreetView [6] or Places [49] to process object removal on real images. Please refer to Fig. 17 for results. These real world images are complex for large area of distractors and complicated background. However, our model can handle them well, which indicates the effectiveness, applicability and generality of our model.

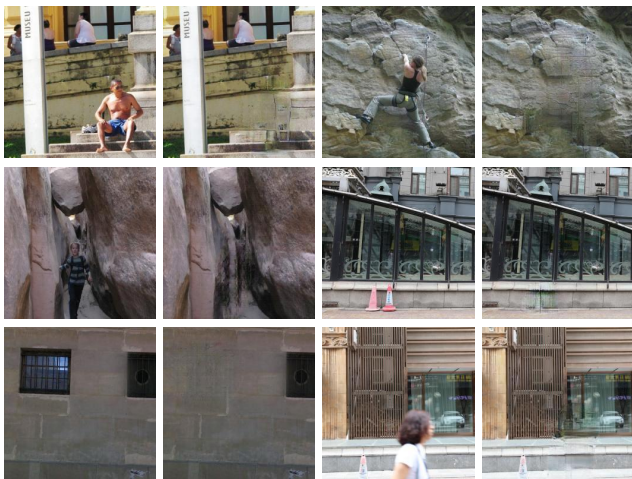
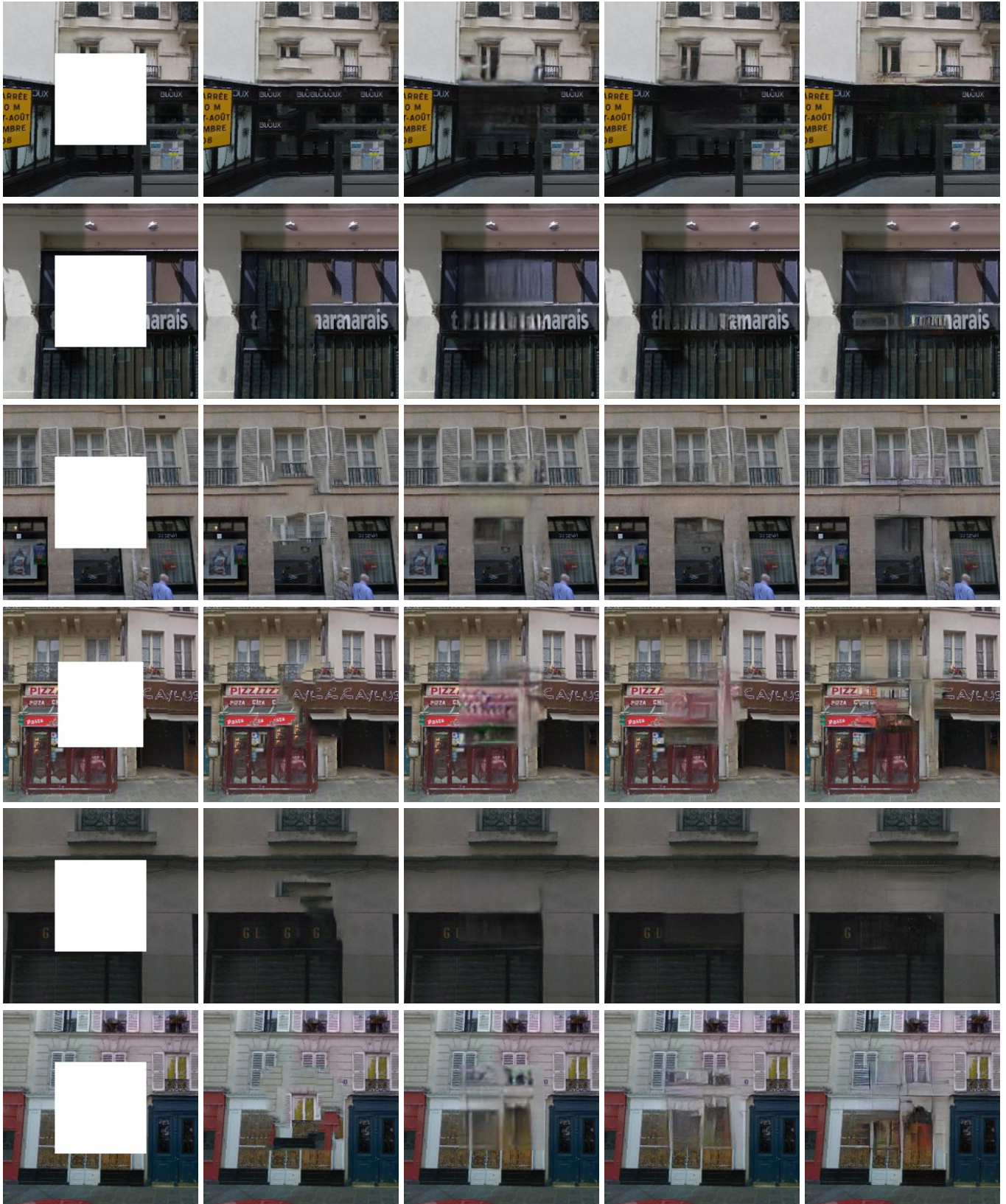
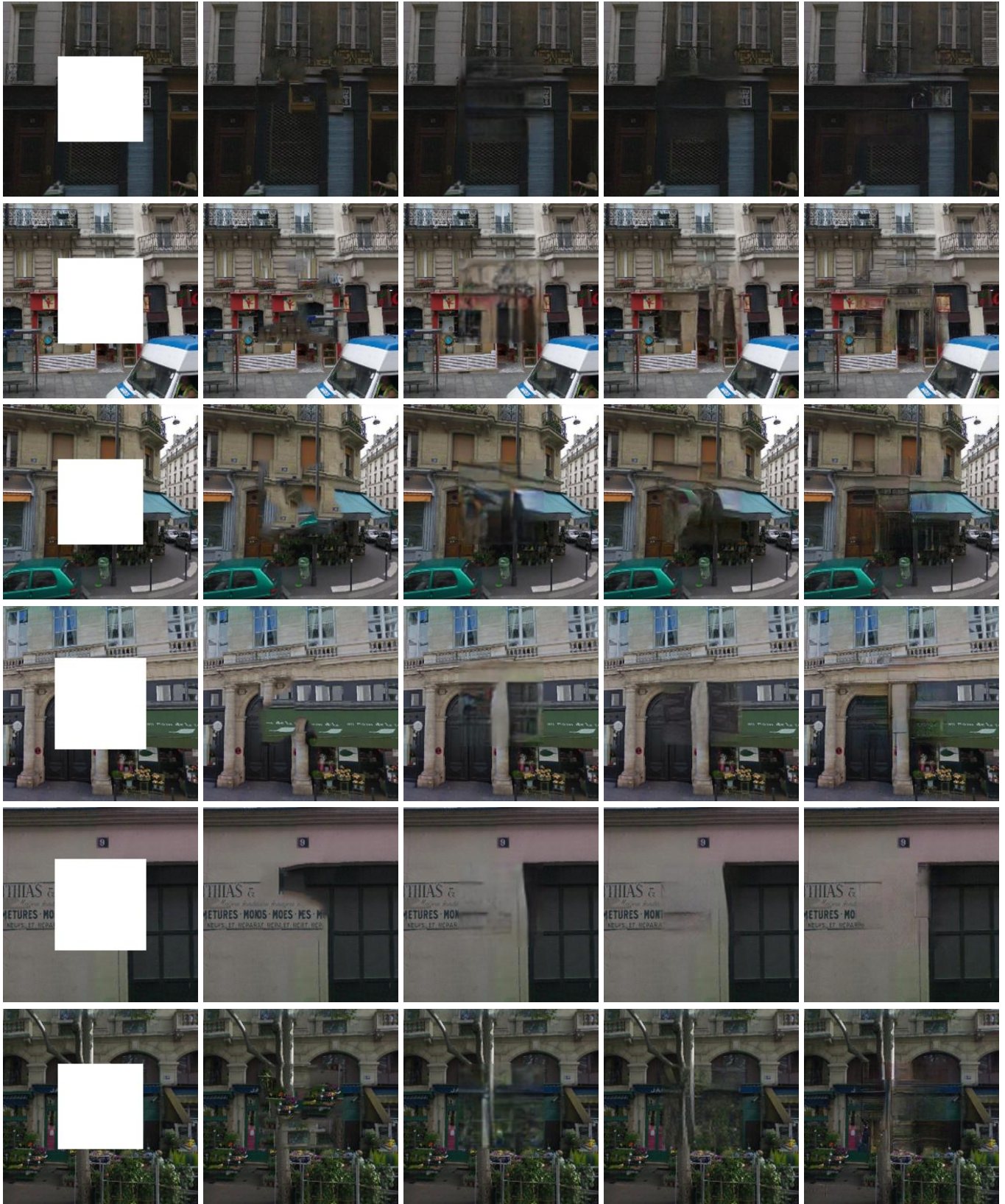


Figure 17: Object removal on real images.



Input                      Content-Aware Fill [1]                      Context Encoder [31]                      MNPS [47]                      Ours

Figure 14: More comparisons on the Paris StreetView dataset. All images are scaled to  $256 \times 256$ .



Input                      Content-Aware Fill [1]                      Context Encoder [31]                      MNPS [47]                      Ours

Figure 15: Comparisons on the Paris StreetView dataset. All images are scaled to  $256 \times 256$ .

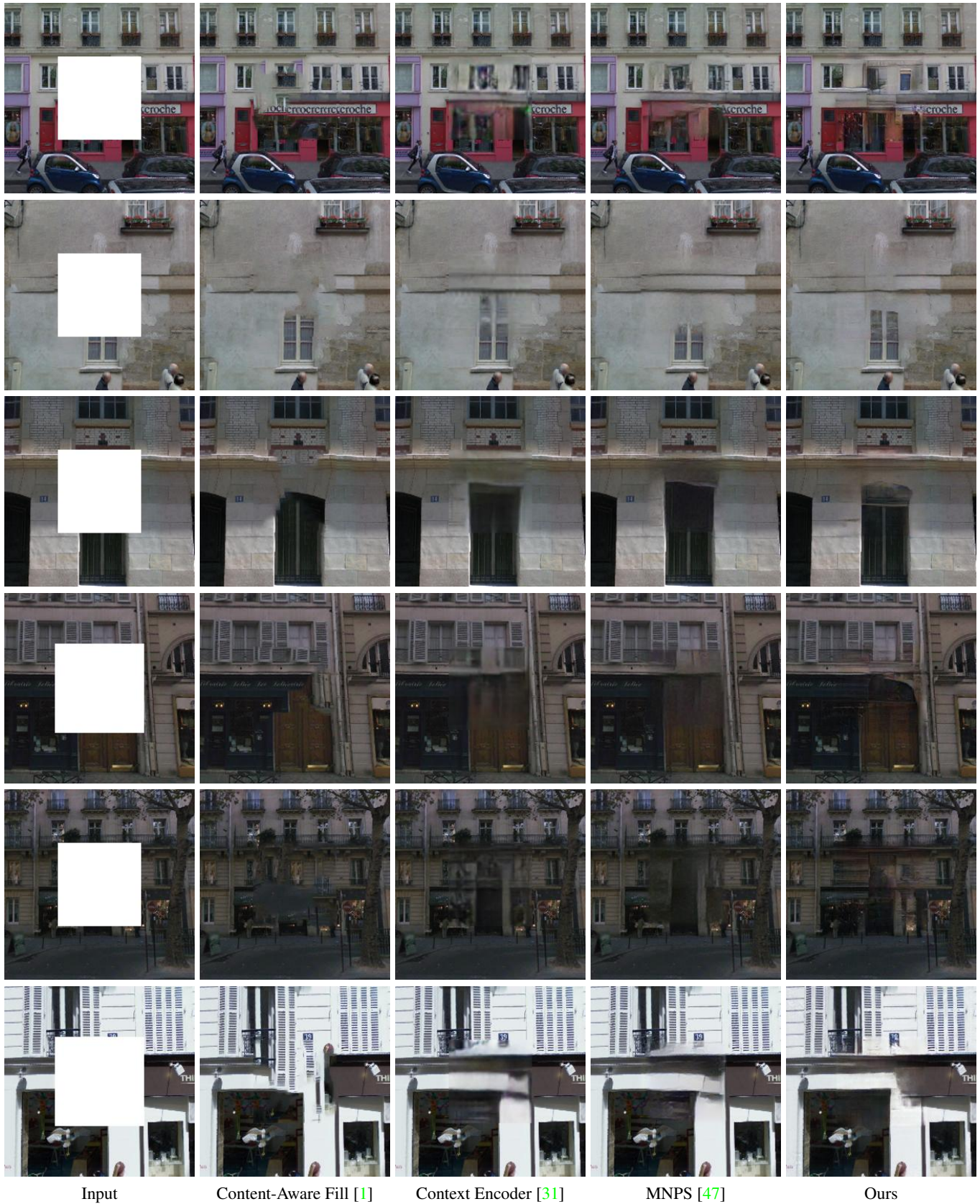


Figure 16: Comparisons on the Paris StreetView dataset. All images are scaled to  $256 \times 256$ .